A&A 433, 205–216 (2005)
DOI: 10.1051/0004-6361:20042143

Astronomy & Astrophysics

High spatial resolution radio continuum observations of compact H II regions in the Magellanic Clouds

N. L. Martín-Hernández[1], R. Vermeij[2], and J. M. van der Hulst[2]

[1] Observatoire de Genève, 51 chemin des Maillettes, 1290 Sauverny, Switzerland
e-mail: leticia.martin@obs.unige.ch
[2] Kapteyn Astronomical Institute, PO Box 800, 9700 AV Groningen, The Netherlands

Received 8 October 2004 / Accepted 23 November 2004

Abstract. We present high spatial resolution observations of the 6 cm continuum emission of compact H II regions in well-known sites of massive star formation located in the Small and Large Magellanic Clouds. The observations include N81 in the SMC, and N4A, N83B, N11A, N160A and N159-5 in the LMC. Some of the compact H II regions are isolated, while others are embedded in more diffuse ionised regions. A description of the radio morphology of the sources, together with comparisons with other observations, is given in detail. The regions cover a wide range in size (from ~0.1 to 7 pc), rms electron density (from ~200 to 6500 cm^{-3}), emission measure (from $\sim 3 \times 10^5$ to 2×10^7 pc cm^{-6}), ionised gas mass (from ~0.2 to 750 $M_\odot$) and rate of Lyman continuum photons (from $\sim 3 \times 10^{47}$ to 5×10^{49} s^{-1}). The spectral types determined from the Lyman continuum fluxes are consistent with optical determinations. We have compared these Magellanic Cloud H II regions with their Galactic counterparts in terms of size, rms electron density and Lyman continuum flux. This comparison shows that their properties relate to each other in the same way as those in Galactic H II regions.

Key words. radiation mechanisms: thermal – stars: formation – ISM: H II regions – galaxies: Magellanic Clouds – radio continuum: ISM

1. Introduction

Massive stars are a dominant force in the evolution of the interstellar medium of galaxies. Through their strong stellar winds, ultraviolet radiation and violent supernova explosions, massive stars are responsible for a large amount of the momentum and kinetic energy input into the interstellar gas. Moreover, these hot stars emit a large part of their energy at extreme ultraviolet (EUV) wavelengths. These EUV photons can couple well to the surrounding gas through ionisation of hydrogen atoms forming H II regions. These H II regions can also influence their surroundings dynamically. The high pressure of the ionised gas drives shock waves, sweeping up the ambient molecular cloud and triggering the formation of new stars. Understanding the characteristics of massive stars and their interaction with their environment is therefore a key problem in astrophysics.

Ultracompact H II (UCH II) regions represent the earliest phase in which the newly born massive star can be detected by its ionising radiation. In the UCH II phase, the accretion has likely stopped and the young star is clearing out its environment, starting to create a small region of ionised gas detectable at radio wavelengths. These UCH II regions might evolve further into compact (C) and giant H II regions when the dense, ionised gas expands into the surrounding molecular gas.

Radio continuum surveys of Galactic UCH II and CH II regions with high angular resolution have been made with the *Very Large Array* (VLA) (e.g. Wood & Churchwell 1989; Fich 1993; Garay et al. 1993; Kurtz et al. 1994; Afflerbach et al. 1996; Rudolph et al. 1996; Kurtz et al. 1999; Kim & Koo 2001) and the *Australia Telescope Compact Array* (ATCA) (e.g. Martín-Hernández et al. 2003). These observations at centimetre wavelength have proved useful in tracing the free-free emission emitted by the densest compact ionised regions, still deeply enshrouded and inaccessible in the optical.

Radio observations using the ATCA can as well be useful to trace the early stages of star formation in the nearby Large and Small Magellanic Clouds (LMC and SMC, respectively). At the typical spatial resolution of the ATCA (1″–2″), these observations can provide a unique insight into the densest regions of massive star forming sites on spatial scales of 0.2–0.5 pc. With this aim in mind, we have conducted observations of compact H II regions in the Magellanic Clouds with high spatial resolution at 6 cm using the ATCA. Our sample consists of well-known sites of massive star formation which have been selected from the *Infrared Space Observatory* (ISO) sample by Vermeij et al. (2002). These sources where originally selected for their bright infrared emission and relatively simple geometry. Consequently, many of the objects in the sample are

Table 1. Summary of ATCA observations. The object name, pointing coordinates (J2000.0), angular size (θ) and position angle (PA) of the restoring beam, rms noise and a list of other source designations are given.

Target object	Pointing coordinates RA ($^{h\,m\,s}$)	Dec ($^\circ\ '\ ''$)	Restoring beam $\theta(''x'')$	PA ($^\circ$)	σ (mJy/beam)	Other source designations*
N81	01 09 12	−73 11 42	2.18 × 1.66	−43.0	0.14	IC 1644, SMC-DEM138
N4A	04 52 06	−66 55 24	2.06 × 1.77	8.3	0.05	NGC 1714, LMC-DEM8b, SL64, ESO 85EN08, KMHK168
N83B	04 54 24	−69 11 00	1.91 × 1.60	−3.4	0.16	NGC 1748, IC 2114, LMC-DEM22c, ESO 56EN24
N11A	04 57 18	−66 23 16	1.88 × 1.65	7.0	0.09	IC 2116
N160A	05 39 42	−69 38 54	2.03 × 1.78	−6.8	0.56	NGC 2080, SL641, ESO 57EN12, BRHT18b
N159-5	05 40 00	−69 44 36	1.90 × 1.61	−16.6	0.59	

* Other designations listed in the catalogues by Bica & Schmitt (1995) and Bica et al. (1999). References to acronyms: SL = Shapley & Lindsay (1963); LMC-DEM = Davies et al. (1976); KMKH = Kontizas et al. (1990); BRHT = Bhatia et al. (1991).

bright, highly excited compact blobs (HEBs), of which several have been discovered in the Magellanic Clouds in the last two decades (e.g. Heydari-Malayeri & Testor 1982). These HEBs are usually only a few arcsec across and are thought to be the first step in the evolution from an UCH II region towards more extended structures.

Some of our observations have been already presented by Indebetouw et al. (2004) as part of a larger sample. Here, however, we present a systematic description of the sources with estimates of the physical properties of the ionised gas (such as the opacity, rms density, emission measure, total mass of ionised hydrogen, excitation parameter and Lyman continuum photon flux) derived from the thermal radio fluxes. A comparison of these physical properties with those of their Galactic counterparts is also shown. Contrary to the images presented by Indebetouw et al. (2004), our observations include the shorter baseline information which provides valuable information on the diffuse structures.

The paper is structured as follows. Section 2 describes the ATCA observations and data reduction. Section 3 presents the contour maps of the observed H II regions. In Sect. 4, estimates of the physical properties of the ionised gas derived from the thermal radio fluxes are given. Detailed descriptions of the morphology and properties of the sources is given in Sect. 5. Section 6 discusses the properties of the sources and a comparison with Galactic H II regions is made. A summary of the results is given in Sect. 7.

2. Observations and data reduction

The objects were observed with the ATCA. The ATCA is an east-west synthesis instrument with 6 22-m antennae on a 6 km track. Five antennae are movable into configurations with baselines between 31 m and 6 km. The data were obtained in snapshot mode during two different runs on 2000 April 8−9 and 2000 May 18−19 in the 6D and 1.5D configurations. The sample objects and pointing coordinates are listed in Table 1. Each object was observed 5 times for 8 min each observing run, so for each object we have an effective integration time of 80 min covering 10 different hour angles, separated by about 18 degrees in hour angle.

The ATCA data were calibrated according to standard techniques using the MIRIAD software package described in *The Miriad User's Guide*[1] (see also Sault et al. 1995). ATCA calibrator sources close to the target objects were used to track the gains and phases of the individual antennas. The flux density scale was calibrated using observations of the compact extragalactic source PKS 1934−638 (the ATCA primary calibrator). PKS 1934−638 has no detectable linear polarisation and therefore can be used to solve for polarisation leakages. The images were formed using the technique of multi-frequency synthesis and uniform weighting with pixel sizes of 0.″3. These images were deconvolved using the SDI CLEAN algorithm (Steer et al. 1984) and restored with the diffraction limited beams. Values for the restoring beams and the rms noise of the final images are summarised in Table 1.

Interferometric observations are limited to angular scales smaller than $\theta = \lambda/(d - D/2)$, where d is the shortest baseline (77 m in the case of our observations) and D is the diameter of a single antenna (22 m for the ATCA). This limits our data to angular scales smaller than $\theta \sim 3'$. The poor u, v sampling with only 10 different hour angles and 2 configurations limits this angular scale even more. This must be taken into account when considering large, extended sources.

The ATCA simultaneously takes 3.6 and 6 cm observations. Both 3.6 and 6 cm images were calibrated. However, due to the poor u, v sampling and the complexity of the sources, the reconstruction of the 3.6 cm images was very difficult and the quality of the final result was very low. Consequently, here we will only present the 6 cm observations.

Each image was analysed in the following way. The peak flux densities and coordinates of the different components were determined using the task *maxfit* in MIRIAD. In the case of large, extended structures, the integrated flux densities were obtained by integrating within the 3σ contour using the task *ellint*, while their sizes were determined using the task *imfit* and fitting an elliptical or circular disc. These flux densities must be considered as lower limits because of the poor u, v sampling of the data. In the case of compact objects, the integrated flux densities and sizes were determined by fitting a Gaussian using the task *imfit*. We estimate that the uncertainties in these

[1] http://www.atnf.csiro.au/computing/software/miriad

Table 2. Peak coordinates, peak flux densities, integrated flux densities, and sizes derived from the 4.8 GHz continuum images. The listed positions correspond to the location of the peak of each feature. The sizes have been determined by fitting a circular or elliptical disc (d) or a Gaussian (g).

Object[◇]	Peak coordinates RA (h m s)	Dec (° ′ ″)	Peak S_ν (mJy/beam)	Integrated S_ν [♮] (mJy)	Size[♭] (″)
N81	01 09 12.464	−73 11 39.08	3.5	37.0	11.7×7.5, 74.6° (d)
N4A−1	04 52 09.414	−66 55 23.82	3.9	231.0	35.4×21.8, −53.3° (d)
N83B−1	04 54 26.100	−69 11 01.87	22.6	39.1	1.7×1.4, −58.0° (g)
N83A	–	–	–	247.0	49.0×39.4, −3.9° (d)
N83 s	04 53 58.593	−69 11 06.16	2.4	3.2	1.2×0.7, 9.8° (g)
N11A	04 57 16.364	−66 23 19.09	2.9	20.0	6.6×5.7, 88.5° (d)
N11B	–	–	–	118.0	Extended
N11 s	04 56 57.274	−66 25 12.83	1.3	1.4	0.68×0.47, 20.8° (g)
N160A	–	–	–	927.0	36.0 (d)
N160 A1	05 39 43.296	−69 38 54.39	19.1	89.2	4.2×3.4, 50.9° (g)
N160 A2	05 39 46.006	−69 38 38.76	47.9	179.8	3.8×3.3, 35.5° (g)
N159#1	05 40 04.357	−69 44 37.54	19.2	116.1	4.8×4.1, −14.1° (g)
N159#4	05 39 37.502	−69 45 26.01	28.2	172.5	4.4×4.1, 5.8° (g)
N159#5	05 39 37.577	−69 46 09.50	9.3	–	Unresolved

[◇] See Sect. 5 for a detailed description of every individual object. [♮] Uncertainties are ∼10%. [♭] The position angle (PA) in degrees is given for most objects.

integrated fluxes, evaluated by comparing the values obtained by using *imfit* and by simply integrating over a box, are not larger than 10%. Peak coordinates, peak and integrated flux densities, and sizes are reported in Table 2.

3. Contour maps

Contour maps of the radio continuum emission at 4.8 GHz are shown in Fig. 2. The contour levels are specified in the figure caption. A detailed description of the sources is given in Sect. 5.

4. Physical properties of the ionised gas

Complicated geometries hamper the determination of important physical parameters such as opacity, electron density and emission measure because the geometry of the source is required. The simplest geometry one can consider is a spherical and homogeneous H II region. Following Panagia & Walmsley (1978), the (rms) electron density of a spherical, optically thin, thermal source can be computed from:

$$\langle n_{\rm e}\rangle = 4.092\times10^{5}\left(\frac{S_\nu}{\rm Jy}\right)^{0.5}\left(\frac{T_{\rm e}}{10^4\ {\rm K}}\right)^{0.25}\left(\frac{D}{\rm kpc}\right)^{-0.5} \times b(\nu,T_{\rm e})^{-0.5}\,\theta_{\rm D}^{-1.5}\ {\rm cm}^{-3}, \quad (1)$$

where S_ν is the integrated flux density in Jy, $T_{\rm e}$ is the electron temperature, D is the distance to the source and $\theta_{\rm D}$ is the source angular diameter in arcsec. The function $b(\nu, T)$ is defined by

$$b(\nu,T_{\rm e}) = 1 + 0.3195\log\left(\frac{T_{\rm e}}{10^4\ {\rm K}}\right) - 0.2130\log\left(\frac{\nu}{\rm GHz}\right), \quad (2)$$

where ν is the frequency of the radio observation. The emission measure, EM, can be derived from the electron density using:

$$EM = \langle n_{\rm e}\rangle^2\, L, \quad (3)$$

where L is the size of the source along the line-of-sight. The expression for EM can be re-written as:

$$EM = 8.118\times10^{8}\left(\frac{S_\nu}{\rm Jy}\right)\left(\frac{T_{\rm e}}{10^4\ {\rm K}}\right)^{0.5}\theta_{\rm D}^{-2}\,b(\nu,T_{\rm e})^{-1}\ {\rm pc\ cm^{-6}}. \quad (4)$$

The optical path length for free-free emission can be derived using the expression given by Mezger & Henderson (1967):

$$\tau_\nu = 8.235\times10^{2}\,a_\nu\left(\frac{T_{\rm e}}{\rm K}\right)^{-1.35}\left(\frac{\nu}{\rm GHz}\right)^{-2.1}\left(\frac{EM}{\rm pc\ cm^{-6}}\right)^{-2.1}, \quad (5)$$

where a_ν is a correction factor near unity whose exact value depends on the frequency ν.

The mass of ionised gas, $M_{\rm H^+}$, can be derived using the relation:

$$M_{\rm H^+} = \frac{4\pi}{3}r\langle n_{\rm e}\rangle m_{\rm H}\left(\frac{1}{1+y}\right), \quad (6)$$

where r is the source radius, $m_{\rm H}$ is the mass of the hydrogen atom and y is the abundance ratio by number of He^+ to H^+. $M_{\rm H^+}$ can be re-written as:

$$\frac{M_{\rm H^+}}{M_\odot} = 6.036\times10^{-4}\left(\frac{T_{\rm e}}{10^4\ {\rm K}}\right)^{0.25}\left(\frac{D}{\rm Kpc}\right)^{2.5} \times\theta_{\rm D}^{1.5}\,b(\nu,T_{\rm e})^{-0.5}\left(\frac{1}{1+y}\right). \quad (7)$$

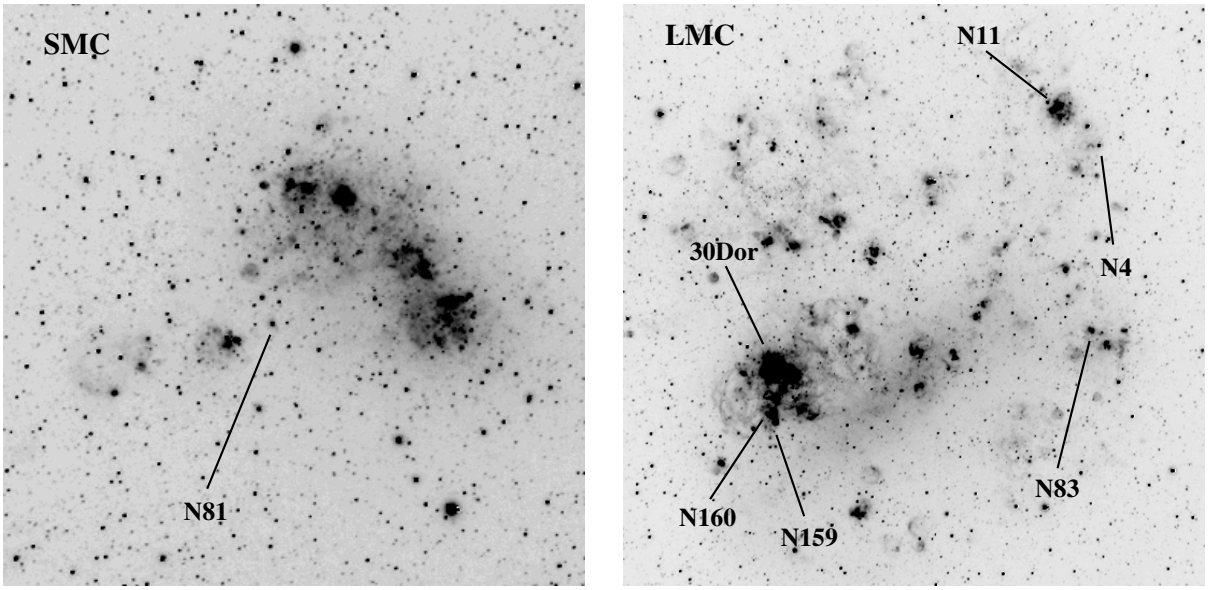

Fig. 1. Arc-minute resolution Hα images of the Small (*left*) and Large Magellanic Clouds (*right*). The H II regions in our ATCA sample are indicated. These images are part of the Southern H-Alpha Sky Survey Atlas (SHASSA).

The excitation parameter, U, can be derived from the relation $U = r\,\langle n_{\rm e}\rangle^{2/3}$, which can be re-formulated as:

$$U = 13.36\left(\frac{S_\nu}{\rm Jy}\right)^{1/3}\left(\frac{T_{\rm e}}{10^4\ {\rm K}}\right)^{1/6}\left(\frac{D}{\rm kpc}\right)^{2/3} \times b(\nu, T_{\rm e})^{-1/3}\ {\rm pc\ cm^{-2}}. \quad (8)$$

Finally, the number of hydrogen ionising photons ($h\nu > 13.6$ eV) per second required to maintain the ionisation of the nebula can be estimated from:

$$N_{\rm Lyc} = \frac{4\pi}{3}\alpha_{\rm B} U^3, \quad (9)$$

where $\alpha_{\rm B}$ is the recombination coefficient for hydrogen, which depends on the the electron temperature. If a power law approximation is assumed for this dependence, we find that $\alpha_{\rm B} \simeq 2.59\times10^{-13}\,(T_{\rm e}/10^4\,{\rm K})^{-0.83}$ cm^3 s^{-1}. Hence, $N_{\rm Lyc}$ can be written as:

$$N_{\rm Lyc} = 7.603\times10^{46}\left(\frac{S_\nu}{\rm Jy}\right)\left(\frac{T_{\rm e}}{10^4\ {\rm K}}\right)^{-0.33}\left(\frac{D}{\rm kpc}\right)^{2} \times b(\nu, T_{\rm e})^{-1}\ {\rm s^{-1}}. \quad (10)$$

This expression assumes that no UV photons have leaked out of the H II region or have been absorbed by internal dust. In either case, the value of the Lyman continuum photon flux derived using the above equation must be considered as a lower limit.

The derived physical parameters (τ_ν, $\langle n_{\rm e}\rangle$, EM, $M_{\rm H^+}$, U and $N_{\rm Lyc}$) of the compact objects are shown in Table 3. They have been computed adopting $T_{\rm e}$ = 14 000 K and y = 0.883 for N81 and $T_{\rm e}$ = 10 000 K and y = 0.090 for the LMC sources (see Sect. 5). We have taken as a representative size of the sources the geometrical average of the major and minor axes listed in Table 2. The adopted distances to the LMC and SMC are, respectively, 50 and 60 kpc (Storm et al. 2004).

5. Description of the sources

5.1. N81

N81 is a high-excitation compact H II blob (HEB) situated in the Shapley Wing (Shapley 1940) well outside the main body of the SMC (see Fig. 1). In contrast to the typical H II regions of the Magellanic Clouds, which are structures extending over several arc minutes and powered by a large number of OB stars, HEBs are very dense and small regions and are, in general, heavily affected by local dust (e.g. Israel & Koornneef 1991). A detailed study of this region in the optical and near-infrared was made by Heydari-Malayeri et al. (1988). They estimated some of its physical characteristics: an age of 1 to 2.5×10^6 yr (derived from the equivalent width of the Hβ emission), an electron temperature of ∼14 000 K (from the optical [O III] 4363, 4959 and 5007 Å lines), an electron density of 420 cm^{-3} (from the [S II] 6717 and 6731 Å lines) and a low metal content typical of the chemical composition of the SMC. High spatial resolution imaging with the *Hubble Space Telescope* (HST) has shown the presence of a tight cluster of massive OB stars embedded in this H II region (Heydari-Malayeri et al. 1999b). Six of these stars are grouped in the core region of ∼2″ diameter. The HST images displayed marks of strong stellar winds, shocks and ionising fronts typical of turbulent massive star forming regions. Far UV spectroscopic observations of the cluster carried on with the *Space Telescope Imaging Spectrograph* (STIS) on the HST revealed features characteristics of an O6–O8 stellar type (Heydari-Malayeri et al. 2002b).

The ATCA map (Fig. 2a) reveals a compact cometary-like region of 11.″7 × 7.″5 (or 3.4 pc × 2.2 pc at the distance of the SMC) exhibiting a compact head towards the west and a tail trailing to the east. This morphology agrees with the interpretation of N81 being an H II region undergoing a champagne-flow (Heydari-Malayeri et al. 1999b), where the bright arc on the west represents the ionisation/shock front advancing in the

Table 3. Physical properties of the sources found in the 4.8 GHz continuum images. Physical parameters include the linear diameter, opacity, rms density, [S II] density, emission measure, total mass of ionised hydrogen, excitation parameter, Lyman continuum photon flux and spectral type.

Object	Diameter† (pc)	τ_ν	$\langle n_e \rangle$ (cm^{-3})	n_e([S II]) (cm^{-3})	EM (10^6 pc cm^{-6})	M_{H^+} ($M_\odot$)	U (pc cm^{23})	log N_{Lyc} (s^{-1})	Sp. type⋆
N81	2.72	0.003	406	420	0.45	56	74.7	49.00	O7V
N4A–1	6.73	0.003	205	130	0.28	745	117.2	49.70	2×O4V
N83B–1	0.37	0.190	6459	700	15.60	4	64.9	48.93	O7V
N83A◇	–	–	–	–	–	–	–	–	–
N83 s	0.22	0.044	4035	–	3.62	0.5	28.2	47.84	09V
N11A	1.49	0.006	583	720	0.50	23	51.9	48.64	O8V
N11B◇	–	–	–	–	–	–	–	–	–
N11 s	0.14	0.051	5510	–	4.16	0.2	21.4	47.48	B0V
N160A◇	–	–	–	–	–	–	–	–	–
N160 A1	0.92	0.072	2545	2000	5.93	23	85.4	49.29	O4V/O5V
N160 A2	0.86	0.166	3983	540	13.62	30	107.8	49.59	2×O4V/O5V
N159#1	1.08	0.068	2282	830	5.60	34	93.2	49.40	O4V
N159#4	1.03	0.110	2970	–	9.08	38	106.4	49.57	2×O4V/O5V
N159#5▷	0.42	0.035	2610	–	2.89	2.4	40.2	48.30	O8V

† Diameter in pc of the homogeneous sphere assumed to be representative of the object. ⋆ Spectral type obtained from N_{Lyc} by using the calibration of Smith et al. (2002). ◇ Extended source. ▷ Properties are derived taking the beam FWHM as the diameter of the source.

molecular cloud, and the tail is ionised gas pouring out into the interstellar medium. The star symbol in Fig. 2a marks the location of the brightest member of the stellar cluster ionising the nebula (Heydari-Malayeri et al. 1999b). The rate of hydrogen ionising photons estimated from the total radio flux density is 1×10^{49} s^{-1}, which corresponds to an O star with a spectral type of O7V (Smith et al. 2002), in perfect agreement with the spectroscopic spectral type. We note that even though the radio continuum is probably not all generated by a single star (for instance, in this case, N81 is ionised by a cluster of massive OB stars), because of the steep dependence of ionising flux on stellar mass, the spectral type derived in this way gives a good approximation to the spectral type of the most massive star(s).

Recently, Indebetouw et al. (2004) have imaged N81 at 3 and 6 cm using the ATCA in the 6A configuration. They measure a total flux density at 6 cm of 33 ± 1 mJy, which agrees well with the value we quoted here. Their 6 cm contour map is more detailed than ours, although the general morphology is comparable.

5.2. N4A

N4 is an H II complex lying towards the north-west of the LMC (see Fig. 1). N4A is the brightest part of the complex. Around 1′ to the NE of N4A is the fainter H II region N4B, while around 1′ to the NW is the bright star WOH 53, a M supergiant belonging to the LMC (see Fig. 1 by Heydari-Malayeri & Lecavelier Des Etangs 1994). N4A is an H II region of about 1′ × 1′ in Hα formed by two components: N4A–1 and N4A–2. N4A–1 is the brightest component, providing about 60% of the total Hα flux. N4A–2 is a diffuse nebulosity apparently streaming from N4A–1 towards the west. Heydari-Malayeri & Lecavelier Des Etangs (1994) give estimates of several physical properties. From the [O III] 4363, 4959 and 5007 Å lines, they derive an electron temperature of ∼9400 K; from the [S II] 6717 and 6731 Å lines, an electron density of 130 cm^{-3}; chemical abundances are in good agreement with the average LMC values.

The ATCA map of N4A (see Fig. 2b) shows only detectable radio emission towards N4A–1, with a size of about 35″ × 22″, or 8.5 pc × 5.3 pc at the distance of the LMC. The radio morphology, characterised by a sharp front to the east and north, agrees very well with that in Hα. Two stars lying in the central part of N4A–1 (their approximate position are indicated in Fig. 2b) are suspected to be the main exciting sources of N4A. Optical spectroscopic observations towards these stars (Wilcots 1994b) reveal He II absorption features suggestive of mid-O type stars. The rate of hydrogen ionising photons estimated from the total radio flux density is 5×10^{49} s^{-1}. According to the new spectral classification of O stars (e.g. Smith et al. 2002), this value is too high to correspond to a unique O star. Two O4V stars, e.g., can account for this Lyman continuum photon flux.

The 6 cm contour map of N4A–1 by Indebetouw et al. (2004) shows only the densest ionised gas towards the NE of the nebula, with a flux density of 27 ± 10 mJy. This source has been also imaged using the ATCA in the 1.5 km configuration by Wilcots (1994a), who quoted a flux density at 6 cm of 250 ± 25 mJy, in perfect agreement with the value we obtain here.

5.3. N83B

The giant H II complex N83 lies in the western part of the LMC (see Fig. 1). It is composed by several ionised gas regions and linked to an OB association (LH5) spanning over

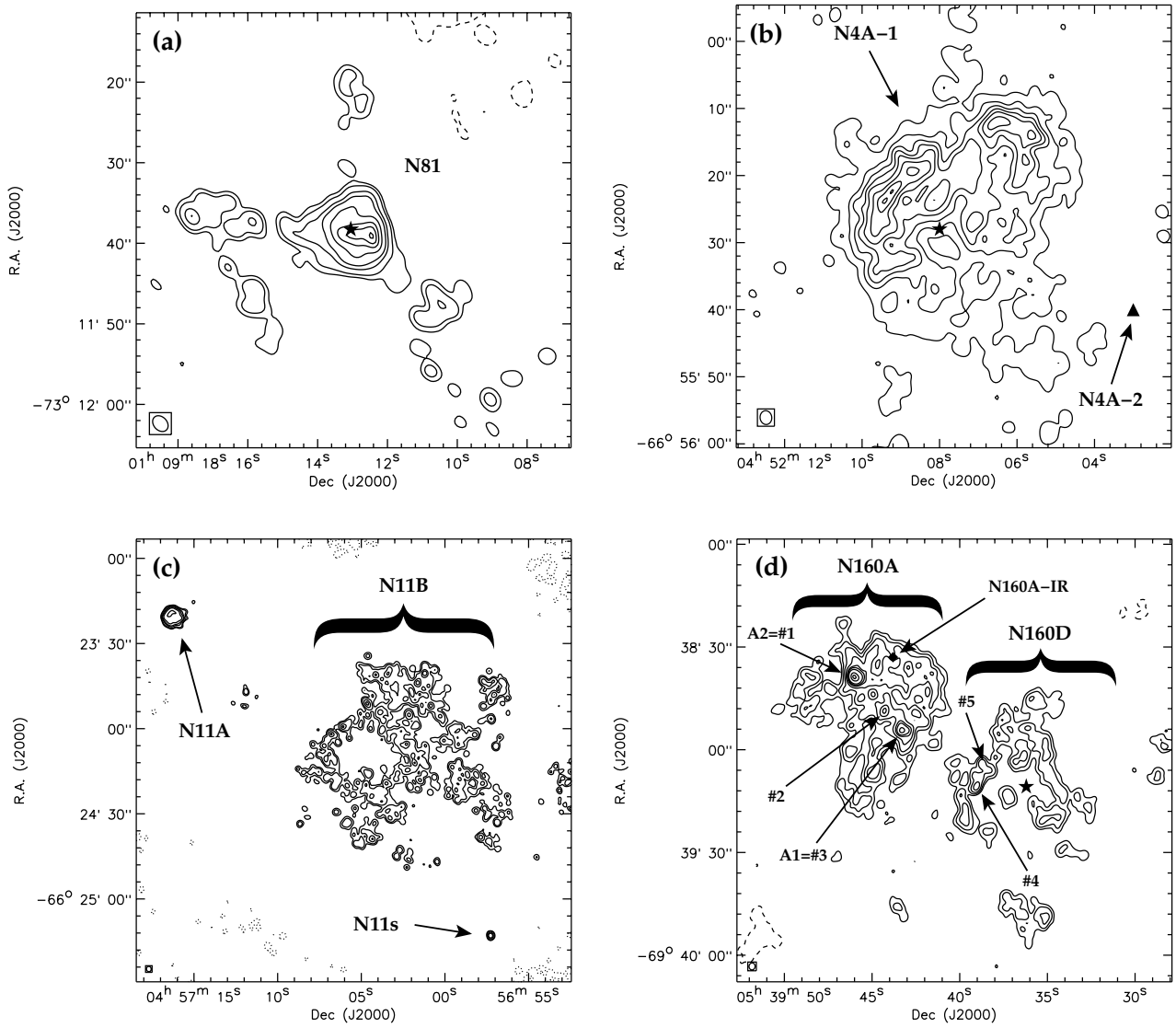

Fig. 2. a) Contour map of N81. Contour levels are −2, 2, 3, 6, 9, 15, 20, 23 and 25 times the image rms σ = 0.14 mJy/beam. The star symbol marks the location of the brightest member of the stellar cluster ionising the nebula (Heydari-Malayeri et al. 1999b). **b)** Contour map of N4A. Contour levels are −2, 2, 9, 18, 27, 36, 48, 60 and 70 times the image rms σ = 0.05 mJy/beam. The radio continuum emission coincides with the bright optical component N4A−1. The approximate location of the diffuse optical component N4A−2 is indicated by a triangle. The star marks the location of two bright stars (Wilcots 1994b) which are probably the exciting sources of the nebula. **c)** Contour map of N11A and N11B. Contour levels are −2, 2, 3, 6, 9, 15 and 30 times the image rms σ = 0.09 mJy/beam. **d)** Contour map of N160A and N160D. Contour levels are −2, 2, 3, 5, 9, 15, 30, 60 and 80 times the image rms σ = 0.56 mJy/beam. Radio continuum emission traces the optical nebulae N160A and N160D. The two bright components in N160A correspond to the HEBs A1 and A2 (Heydari-Malayeri et al. 2002a), which are sources #3 and #1 in Indebetouw et al. (2004). Sources #2, #4 and #5 in Indebetouw et al. (2004) are also marked. The position of the YSO N160A-IR (Henning et al. 1998) is marked by a diamond. The position of the Wolf-Rayet star responsible for the shell structure of N160D, BAT99 124, is indicated by a star (Breysacher et al. 1999). In all panels, the inset on the lower left corner shows the FWHM of the synthesized beam. Negative contours (if present) are indicated by dotted lines.

16 square minutes (see Fig. 1 by Heydari-Malayeri et al. 2001b, where the ionised components of N83 and some stars of the OB association are labelled.). A study by Heydari-Malayeri et al. (1990) detected the presence of a HEB (N83B–1) in the eastern part of component N83B. New HST images by Heydari-Malayeri et al. (2001b) confirmed the presence of this compact object of ∼2.8″ across and detected an even smaller blob (N83B–2) of ∼1″ in diameter lying less than 4″ SW of N83B–1. The whole ionised region N83 covers ∼30″ in Hα and displays a shell structure and a turbulent environment typical of newborn massive star formation sites. The colours of the brightest star situated towards N83B–1 indicate a main sequence O6 star. The work by Heydari-Malayeri et al. (1990) investigated several physical characteristics towards N83B–1 such as the electron temperature (about 10 000 K, obtained from the [O III] 4363, 4959 and 5007 Å lines), electron density (700 cm^{-3}, from the [S II] 6717 and 6731 Å doublet), chemical composition (compatible with the LMC average values) and

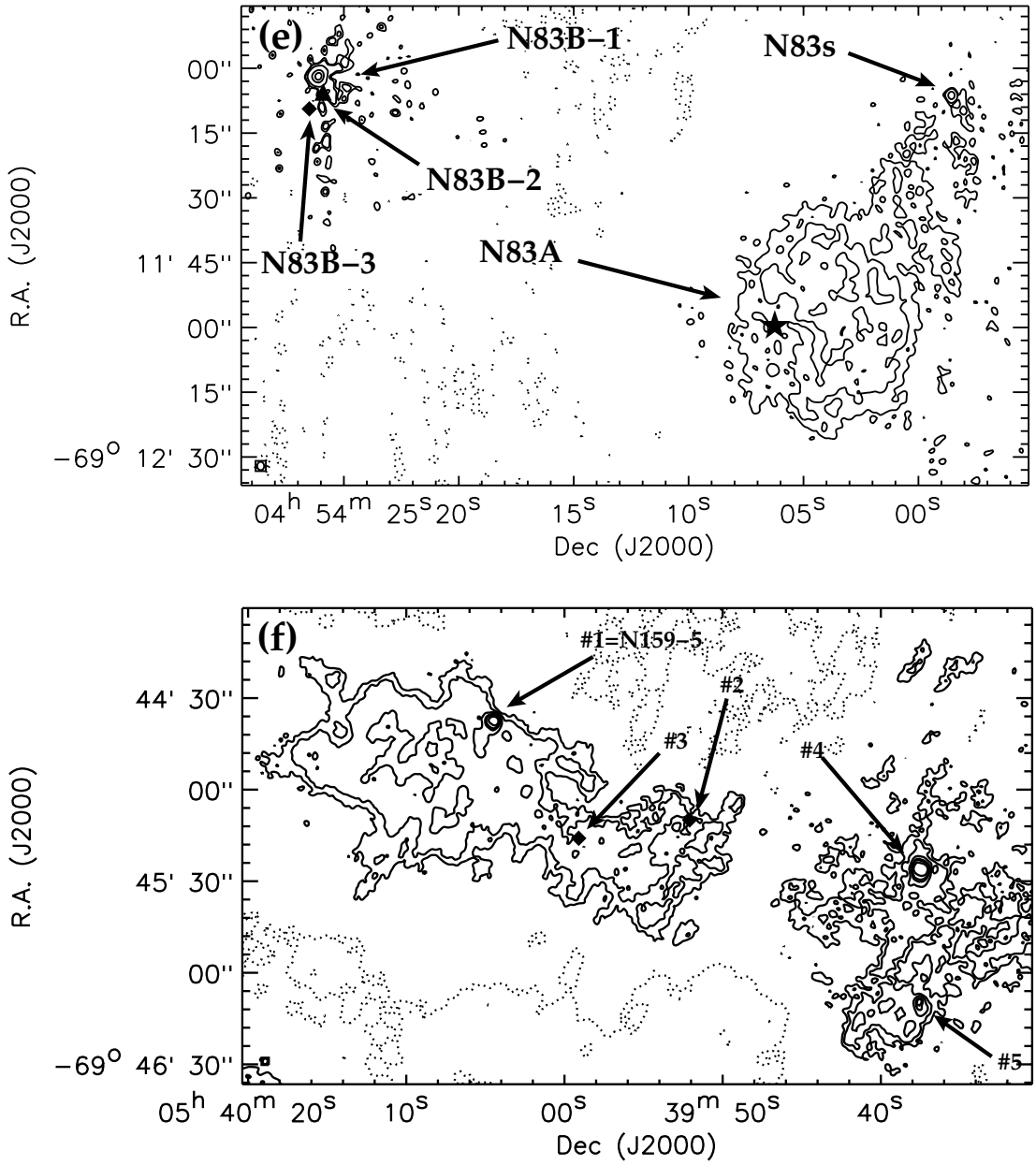

Fig. 2. continued. **e)** Contour map of N83A and N83B. Contour levels are −2, 2, 3, 9, 50 and 100 times the image rms σ = 0.16 mJy/beam. The compact radio source on the top left corner coincides with the HEB N83B−1. The positions of the HEB N83B−2 and the ionised region N83B−3, just south of N83B−1, are indicated by a triangle and a diamond, respectively. The star marks the position of the main exciting star of N83A, Sk-69°25. **f)** Contour map of N159. Contour levels are −2, 2, 3, 5, 9, 12 and 20 times the image rms σ = 0.59 mJy/beam. The three brightest compact sources are object #1 (which corresponds to the HEB N159−5), object #4 and object #5 in Hunt & Whiteoak (1994). Other radio peaks (#2 and #3) found by Hunt & Whiteoak (1994) are indicated by diamonds. Extended radio emission is found around the position of N159A. In all panels, the inset on the lower left corner shows the FWHM of the synthesized beam. Negative contours are indicated by dotted lines.

age (around 4×10^6 yr, inferred from the equivalent width of Hβ).

The ATCA map (Fig. 2e) reveals a strong, high-density (the estimated rms density is ~6500 cm^{-3}), compact source (~1.5″ in diameter, practically unresolved) coinciding with the location of N83B–1. The rate of hydrogen ionising photons estimated from the total radio flux density is 8.5×10^{48} s^{-1}, which corresponds to an O star with a spectral type of O7V (Smith et al. 2002), only slightly later than the photometric spectral type.

The ATCA observations also reveal diffuse radio continuum emission across ~45″ towards the N83A component (also named NGC 1743, SL 87, ESO 56EN21) with a total integrated flux density of 247 mJy and a Lyman photon flux of about 5.4×10^{49} s^{-1}. An unresolved object (labelled N83s) is found NW of N83A, which, if located at the distance of the LMC, could be ionised by an O9V star.

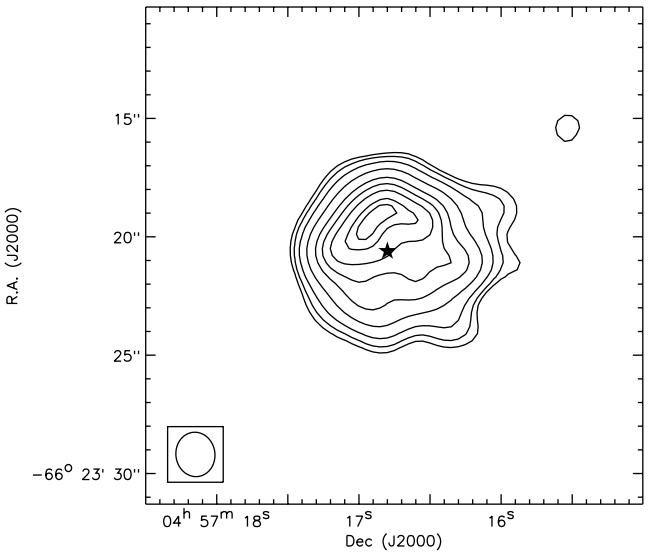

Fig. 3. Close-up of N11A. Contour levels are −2, 2, 3, 5, 9, 15, 20, 25, 30 and 32 times the image rms σ = 0.09 mJy/beam. The star indicates the position of the main exciting star of the region (star #7 in Heydari-Malayeri et al. 2001a). The inset on the lower left corner shows the FWHM of the synthesized beam.

Indebetouw et al. (2004) have recently imaged N83 using the ATCA. They detect two compact sources, one coincident with N83B, labelled B0454−6916(E), and the second, B0454−6916(W), much fainter, which corresponds with N83s. They quote flux densities at 6 cm of 39 ± 1 and 3.6 ± 0.5 mJy, respectively. These values agree perfectly with ours. Their 6 cm image does not show radio emission associated with N83A.

5.4. N11A

The giant complex N11 is the second largest nebula in the LMC after 30 Doradus and lies at the north-western extremity of the LMC bar (see Fig. 1). A dozen nebulae (named N11A to N11L), filaments and voids form the complex (see Fig. 1 by Rosado et al. 1996). A central hole of about 25′ by 20′ is surrounded by several filaments and by the bright cores N11B and C, the knots N11A and D, and the weaker H II regions N11F and I. The other H II regions are located farther away from the central hole. The complex harbours tens of hot stars at different stages of evolution distributed in four OB associations: LH 9, LH 10, LH 13 and LH 14 (Lucke & Hodge 1970). The ATCA observations (see Figs. 2c and 3) were centred on the knot N11A, but they also registered the larger H II region N11B.

N11A is a HEB situated NE of N11B. HST observations (Heydari-Malayeri et al. 2001a) resolve N11A into a very bright core surrounded by a diffuse envelope of about 8″ in diameter. The nebula presents fine structure filaments and a sharp ridge that borders the core along the NE direction. Beyond this ridge, the Hα emission drops by about a factor of 10. A small cluster of five tightly packed stars are seen towards a cavity in the central region. The visual magnitude of the brightest star in the cluster corresponds to an O9V according to the calibration of Vacca et al. (1996) for Galactic stars. The work by Heydari-Malayeri & Testor (1985) derived several physical properties towards N11A such as the electron temperature (∼9400 K, obtained from the [O III] 4363, 4959 and 5007 Å lines), electron density (720 cm^{-3}, from the [S II] 6717 and 6731 Å doublet) and chemical composition (compatible with the LMC average values). The 6 cm map (see Fig. 3) reveals a morphology well in agreement with that seen in the optical. The rate of hydrogen ionising photons estimated from the total radio flux density is 4.4×10^{48} s^{-1}, which corresponds to an O star with a spectral type of O8V (Smith et al. 2002), slightly earlier than the spectral type (O9V) obtained for the brightest star in the ionising cluster. It might be that the radio flux is not entirely dominated by a single O9V star.

Seen in the optical, N11B (also named NGC 1763; Bica et al. 1999) is a bright nebula which surrounds the OB stellar association LH 10, which seems to be the youngest association embedded inside N11 (Parker et al. 1992). Based on a 4′ resolution radio continuum map of McGee et al. (1972) at 6 cm, Israel (1980) estimated a flux density of 1.8 Jy for N11B. This value is much bigger than the 0.118 Jy we obtained by integrating our ATCA map, which indicates that our observations are resolving out a large fraction of the nebula. In fact, the ATCA contours indicates a patchy structure with multiple radio peaks. A particularly bright, high density point source is seen south of N11B (labelled N11s), which, if located at the distance of the LMC, could be ionised by a B0V star.

N11A has been also recently imaged with the ATCA by Indebetouw et al. (2004). These authors detect radio emission towards both regions A and B. Their 3 cm contour image of N11A, which they label B0456−6626(E), agrees very well with the morphology shown in Fig. 3. They quote a 6 cm flux density of 31 ± 5 mJy, slightly higher than the value we obtain (20 mJy). Towards N11B, they find some irregular emission associated with the optical nebula. They also register the presence of N11s, which they denominate B0456−6629(W1), with a 6 cm flux density of 3.3 ± 0.4, again higher than the value we quote (1.4 mJy).

5.5. N160A

N160 (other designations are DEM 284 – Davies et al. 1976 – and MC 76 – McGee & Milton 1966) is a giant H II complex lying about 30′ south of 30 Doradus (see Fig. 1). The complex is formed by two main regions ∼3.5′ apart (Heydari-Malayeri & Testor 1986). The brighter western region comprises components A (NGC 2080) and D (NGC 2077), while the eastern region is formed by components B (NGC 2085) and C (IC 2145). N160 is linked with the OB star association LH 103 (Lucke & Hodge 1970).

N160A is the brightest component of N160 and it is a particularly interesting region since it harbours two HEBs embedded within N160A (called A1 and A2 and discovered by Heydari-Malayeri & Testor 1986) and a young stellar object discovered using near- and mid-IR photometry by Epchtein et al. (1984). This YSO (N160A-IR) has been further observed in the *K*-band and mid-IR by Henning et al. (1998). HST observations (Heydari-Malayeri et al. 2002a) of N160A reveal a

bright nebula of about 35″ by 25″. Three bright star clusters are identified within the nebula along with the two blobs A1 and A2. The compact H II region A1, which is the brightest part of N160A, shows a tiny cavity of some 2.″3 across which might be the result of the strong wind of a bright star found towards the centre of the blob. This star must be a massive O type since it has carved the cavity and produces the hightest [O III]/Hβ ratio in the whole region. The other HEB, A2, is 3″ in diameter, has a patchy appearance marked by the presence of several thin absorption lanes and contains about dozen rather faint stars. The three star clusters seem to ionise N160A. The visual magnitude of the brightest member of the central cluster agrees with an O6.5V star.

The radio continuum emission observed towards N160A by the ATCA (see Fig. 2d) reveals an extended structure of about 36″ where the two HEBs A1 and A2 stand out as two strong radio peaks. As expected from its youth, the YSO (its position is indicated in the figure by a diamond) does not have associated radio continuum emission. The rates of hydrogen ionising photons estimated from the total radio flux densities towards A1 and A2 are 1.9×10^{49} s^{-1} and 3.9×10^{49} s^{-1} respectively. In the case of A1, this corresponds to a main-sequence O star with a spectral type of O4V/O5V (Smith et al. 2002). The $N_{\rm Lyc}$ value obtained for A2 is too high to correspond to a unique O star. Two O4V/O5V stars, e.g., can account for it.

The ATCA observations were centred on N160A, but they also registered radio continuum emission towards N160D. The 6 cm emission traces a bubble structure also revealed in the optical. This bubble or shell may be due to the Wolf-Rayet star BAT99 124 (its position is indicated in the figure by a star symbol), first detected by Morgan & Good (1985).

The work by Heydari-Malayeri & Testor (1986) derived several physical properties towards N160A and D such as the electron temperature (~9900 K for A1 and 9600 for A2, obtained from the [O III] 4363, 4959 and 5007 Å lines), electron density (2000 cm^{-3} for A1, 540 cm^{-3} for A2 and 100 cm^{-3} for D, from the [S II] 6717 and 6731 Å doublet) and chemical composition (compatible with the LMC average values).

The recent ATCA observations by Indebetouw et al. (2004) detect 5 compact radio sources near N160A. Two of them (their sources #3 and #1) coincide with N160 A1 and A2. They quote 6 cm flux densities of 50 ± 5 and 130 ± 7, respectively, lower than the values we obtain. Since the Indebetouw et al. radio image resolve out the diffuse emission around A1 and A2 and we do not, it is likely that our flux densities are contaminated by this low density gas. Their source #2 coincides with a secondary peak within N160A, while sources #4 and #5 correspond to density enhancements in the shell-like structure associated with N160D (see Fig. 2d).

5.6. N159–5

N159 (other designations are MC77 and LH105) is a giant H II complex in the LMC lying about 35′ south of 30 Doradus and very close to N160. In fact, N159 and N160, together with N158 (see Fig. 1), form an impressive chain of H II regions extending southwards from 30 Doradus. N159 is associated with one of the most important concentrations of molecular gas in the LMC (e.g. Johansson et al. 1998) and has many characteristics of typical active star forming regions such as compact H II components, bright infrared emission including infrared protostars, an X-ray source, masers, etc. N159 is basically composed by an oval nebulosity of about 50″ by 35″ (N159A, also denominated NGC2079) and a large and patchy complex which extends over several arcminute to the NE (see Fig. 1 in Heydari-Malayeri & Testor 1982). HST images of this complex (Heydari-Malayeri et al. 1999a) show a very turbulent medium where a large number of filaments, arcs and fronts are visible. Within this complex, Heydari-Malayeri & Testor (1982) discovered a HEB of about 6″ (N159–5) at the edge of a prominent absorption lane running westward into N159. N159–5 has been resolved by the HST (Heydari-Malayeri et al. 1999a). N159–5 shows an overall shape reminiscent of a butterfly, with two distinct ionised lobes separated by ~2.3″. The work by Heydari-Malayeri & Testor (1985) derived several physical properties towards N159–5 such as the electron temperature (~10 500 K, obtained from the [O III] 4363, 4959 and 5007 Å lines), electron density (830 cm^{-3}, from the [S II] 6717 and 6731 Å doublet) and chemical composition (compatible with the LMC average values).

The ATCA observations towards N159–5 reveal it to be a strong compact source of ~4.5″ located in the northern edge of a low brightness region which extends ~3′ from the NE to the SW (see Fig. 2f). This low brightness emission coincides with the absorption lane that crosses N159 and is associated with the molecular cloud N159–E (Johansson et al. 1998).

We indicate in the figure the positions of the radio peaks found by Hunt & Whiteoak (1994) in their 6 cm observations made with ATCA with an angular resolution of 7.″4 × 8.″3. We do not find radio peaks at the positions of their sources #2 and #3. Their radio peak #1 coincides with N159–5, while the positions of #4 and #5 correspond to two bright compact objects we see towards the SW. These two compact regions and the associated low brightness gas form part of the component N159A. N159–5 and #5 correspond to sources LI-LMC 1518 and LI-LMC 1501 W, two bright point sources observed by ISOCAM at 15 μm (Comerón & Claes 1998). Another bright 15 μm point source located ~2″ to the east of LI-LMC 1501 W (LI-LMC 1501 E) does not have a clear radio counterpart.

The rate of hydrogen ionising photons estimated from the total radio flux density measured for N159–5 is 2.5×10^{49} s^{-1}, which can be produced by a single O star with a spectral type of O4V (Smith et al. 2002). The radio flux measured towards #4 can be produced by two O4V/O5V stars. Source #5 could be ionised by an O8V star.

Towards N159, Indebetouw et al. (2004) detect the compact radio sources #1, #4 and #5, with respective 6 cm flux densities of 70 ± 15, 120 ± 15 and 30 ± 5 mJy, somewhat different to the values we obtain. This difference stress the presence of diffuse emission around these sources. A comparison between the 3 cm radio image of source #1 (N159–5) by Indebetouw et al. with the HST image by Heydari-Malayeri et al. (1999a) shows that most of the radio continuum emission is associated with the western lobe of the butterfly-like nebula. These authors do not register the extended emission associated with N159.

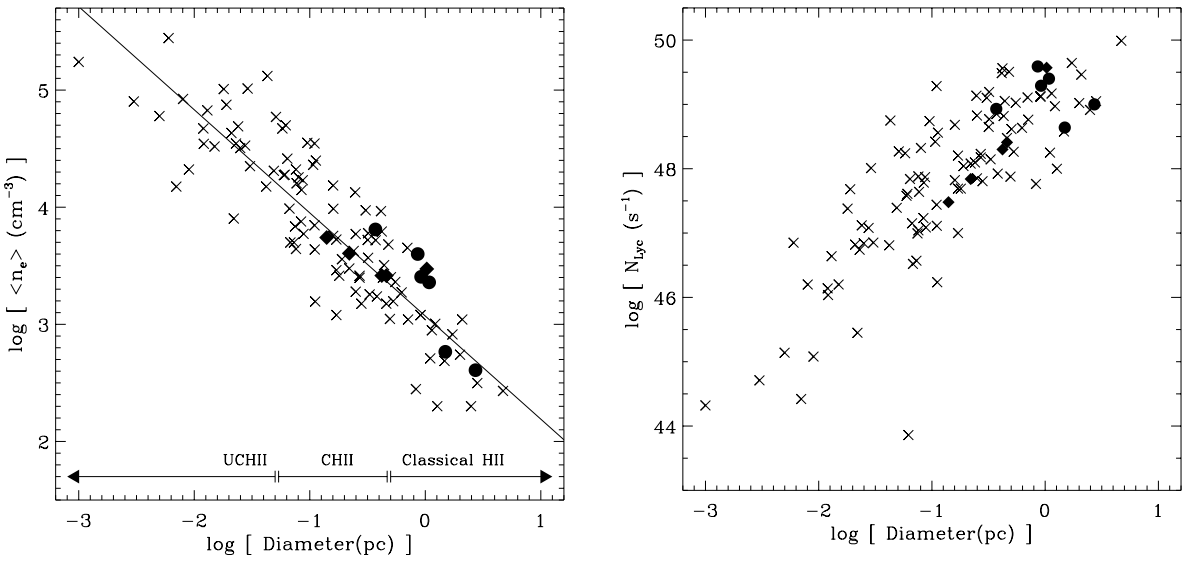

Fig. 4. Plot of the rms electron density (*left*) and Lyman continuum photon flux (*right*) against the linear source diameter. The sample in the Magellanic Clouds is represented by filled symbols: HEBs by circles and the other radio compact sources by diamonds. Crosses represent Galactic H II regions in the samples by Wood & Churchwell (1989), Kurtz et al. (1994) and Martín-Hernández et al. (2003). The typical classification of ultracompact (UC), compact (C) and classical H II regions based on their linear sizes is given at the bottom of the left panel.

6. General properties

The studied H II regions cover a wide range in size (from ∼0.1 to 7 pc), rms electron density (from ∼200 to 6500 cm^{-3}), emission measure (from $\sim 3 \times 10^5$ to 2×10^7 pc cm^{-6}), ionised gas mass (from ∼0.2 to 750 $M_\odot$) and Lyman continuum photon flux (from $\sim 3 \times 10^{47}$ to 5×10^{49} s^{-1}), as shown in Table 3.

If the radio and optical emission sample the same gas and there is no collisional de-excitation, the electron density derived, from instance, from the [S II] 6717 and 6731 Å doublet, n_e([S II]), which reflects the mean of the local density (i.e. the mean density of the clumps), must always be of the same order or greater than the rms density, which is derived by assuming that the emission is uniform along the line of sight. The ratio of both densities then provides the filling factor, which is a measure of how much of the volume of the nebula is filled with clumps. A comparison of the rms densities derived from the 4.8 GHz continuum emission and the densities obtained from the [S II] lines is shown in Table 3. In the case of N81 and N11A, the filling factor we obtain is close to unity, which is not surprising considering the compactness of the emission. However, the rms density derived for the other objects is higher than their respective [S II] densities (up to a factor of 9 in the case of N83B–1). For these cases, the density derived from the [S II] lines is likely representative of a dilute shell surrounding the high-density core traced by the radio emission.

The spectral types determined from the Lyman continuum photon fluxes are consistent with optical determinations.

6.1. A comparison with Galactic H II regions

It is interesting to compare the physical properties derived for the sample of Magellanic Cloud H II regions with those of their Galactic counterparts. This is done in Fig. 4. The left panel shows a plot of the rms electron density against the linear diameter where the Magellanic Cloud H II regions are compared to a large sample of Galactic H II regions compiled from the works by Wood & Churchwell (1989), Kurtz et al. (1994) and Martín-Hernández et al. (2003). Ultracompact and compact H II regions in our Galaxy are known to show a correlation between these two parameters (see e.g. Garay et al. 1993; Garay & Lizano 1999; Martín-Hernández et al. 2003). A least-squares linear fit to the trend observed for the Galactic H II regions gives a slope of -0.88 ± 0.05 and an intercept of 3.07 ± 0.05. The sources in the Magellanic Clouds follow the same relation between density and size. We note that all the observed HEBs (except N11A) fall in the category of compact H II regions, characterised by intermediate sizes ($0.05 < L < 0.5$ pc, where L is the linear diameter) and densities ($10^3 < n_e < 10^4$ cm^{-3}). This supports the idea of HEBs being ionised by young massive stars just leaving their parental molecular cloud.

Assuming that the distribution of spectral types (and hence of the ionisation characteristics) among the stars exciting UCH II and CH II regions is independent of the initial conditions of the surrounding medium, then the rms electron density should be on average proportional to $L^{-3/2}$ (e.g. Osterbrock 1989). However, the observed slope is shallower, what could suggest that, on average, UCH II regions are ionised by stars with lower number of ionising photons (i.e. by later type stars) than those ionising compact and classic H II regions. This hypothesis is supported by the right panel in Fig. 4, which plots the rate of Lyman continuum photons against the diameter. This might imply that UCH II regions are powered by less rich clusters, with a statistically lower chance of having very massive stars. Of course, this is not the only explanation. Several other effects can cause the size-density relation to be shallower than predicted for pure hydrogen Strömgren spheres (see the detailed discussion by Martín-Hernández et al. 2003). For

instance, it could be possible that many UCH II regions are externally ionised objects, corresponding to the densest structures within a larger, inhomogeneous H II region. Optical depth effects and clumpiness, more easily found in UCH II regions than in larger regions, can also shallow the size-density relation since they lead to an underestimate of $N_{\rm Lyc}$. The presence of dust within the ionised gas can also flatten the size-density relation. The larger the dust absorption cross section per H atom, the shallower the relation between $n_{\rm e}$ and D is (the absorption optical depth of dust is $\propto n_{\rm e}^{1/3}$). Consequently, for a particular dust-to-gas ratio, higher densities (as is in the case of UCH II regions) lead to higher dust optical depths and thus, to a higher number of ionising photons absorbed by the dust. Based on the analysis of the size-$N_{\rm Lyc}$, Martín-Hernández et al. (2003) also suggest the possibility that the above interpretation of UCH II regions being excited by later type stars than extended H II regions might just be wrong, and that in fact UCH II regions can be powered by the whole range of O and late B stars.

Wherever the true cause of this relation is, it is clear that the HEBs and the other compact and extended H II regions we have observed in the Magellanic Clouds have physical properties (size, density, luminosity) which relate to each other in the same way as those in Galactic H II regions.

7. Conclusions

We present high spatial resolution observations of the 6 cm continuum emission of compact H II regions in well-known sites of massive star formation located in the Small and Large Magellanic Clouds. The observations include N81 in the SMC, and N4A, N83B, N11A, N160A and N159-5 in the LMC.

Some of the compact H II regions, e.g. N81 and N11A, are isolated, while others are embedded in more diffuse ionised regions. A description of the radio morphology of every source, together with comparisons with other observations, is given in detail.

The H II regions cover a wide range in size (from ∼0.1 to 7 pc), rms electron density (from ∼200 to 6500 cm^{-3}), emission measure (from $\sim 3 \times 10^5$ to 2×10^7 pc cm^{-6}), ionised gas mass (from ∼0.2 to 750 $M_\odot$) and rate of Lyman continuum photons (from $\sim 3 \times 10^{47}$ to 5×10^{49} s^{-1}). The spectral types determined from the Lyman continuum fluxes are consistent with optical determinations. When comparing the rms electron densities with the [S II] densities derived from optical observations, we find that N81 and N11A have a filling factor close to unity, which reflects their compactness of the emission. However, the rms densities derived for the other regions are higher that their respective [S II] densities, indicating that the density derived from the [S II] lines is likely representative of a dilute shell surrounding the high-density core traced by the radio emission.

A comparison with their Galactic counterparts in terms of size, rms electron density and Lyman continuum flux shows that the properties of these SMC and LMC H II regions follow those of the ultracompact, compact and classical H II regions in our Galaxy.

Acknowledgements. We thank the referee for his/her critical reading and constructive comments. This work was supported by the Swiss National Foundation.

References

Afflerbach, A., Churchwell, E., Acord, J. M., et al. 1996, ApJS, 106, 423
Bhatia, R. K., Read, M. A., Tritton, S., & Hatzidimitriou, D. 1991, A&AS, 87, 335
Bica, E. L. D., & Schmitt, H. R. 1995, ApJS, 101, 41
Bica, E. L. D., Schmitt, H. R., Dutra, C. M., & Oliveira, H. L. 1999, AJ, 117, 238
Breysacher, J., Azzopardi, M., & Testor, G. 1999, A&AS, 137, 117
Comerón, F., & Claes, P. 1998, A&A, 335, L13
Davies, R. D., Elliott, K. H., & Meaburn, J. 1976, Roy. Astron. Soc., Mem., 81, 89
Epchtein, N., Braz, M. A., & Sevre, F. 1984, A&A, 140, 67
Fich, M. 1993, ApJS, 86, 475
Garay, G., & Lizano, S. 1999, PASP, 111, 1049
Garay, G., Rodríguez, L. F., Moran, J. M., & Churchwell, E. 1993, ApJ, 418, 368
Henning, T., Klein, R., Chan, S. J., et al. 1998, A&A, 338, L51
Heydari-Malayeri, M., & Lecavelier Des Etangs, A. 1994, A&A, 291, 960
Heydari-Malayeri, M., & Testor, G. 1982, A&A, 111, L11
Heydari-Malayeri, M., & Testor, G. 1985, A&A, 144, 98
Heydari-Malayeri, M., & Testor, G. 1986, A&A, 162, 180
Heydari-Malayeri, M., Le Bertre, T., & Magain, P. 1988, A&A, 195, 230
Heydari-Malayeri, M., van Drom, E., & Leisy, P. 1990, A&A, 240, 481
Heydari-Malayeri, M., Rosa, M. R., Charmandaris, V., Deharveng, L., & Zinnecker, H. 1999a, A&A, 352, 665
Heydari-Malayeri, M., Rosa, M. R., Zinnecker, H., Deharveng, L., & Charmandaris, V. 1999b, A&A, 344, 848
Heydari-Malayeri, M., Charmandaris, V., Deharveng, L., et al. 2001a, A&A, 372, 527
Heydari-Malayeri, M., Charmandaris, V., Deharveng, L., et al. 2001b, A&A, 372, 495
Heydari-Malayeri, M., Charmandaris, V., Deharveng, L., et al. 2002a, A&A, 381, 941
Heydari-Malayeri, M., Rosa, M. R., Schaerer, D., Martins, F., & Charmandaris, V. 2002b, A&A, 381, 951
Hunt, M. R., & Whiteoak, J. B. 1994, Proc. Astron. Soc. Austr., 11, 68
Indebetouw, R., Johnson, K. E., & Conti, P. 2004, AJ, accepted, [arXiv:astro-ph/0407516]
Israel, F. P. 1980, A&A, 90, 246
Israel, F. P., & Koornneef, J. 1991, A&A, 248, 404
Johansson, L. E. B., Greve, A., Booth, R. S., et al. 1998, A&A, 331, 857
Kim, K., & Koo, B. 2001, ApJ, 549, 979
Kontizas, M., Morgan, D. H., Hatzidimitriou, D., & Kontizas, E. 1990, A&AS, 84, 527
Kurtz, S., Churchwell, E., & Wood, D. O. S. 1994, ApJS, 91, 659
Kurtz, S. E., Watson, A. M., Hofner, P., & Otte, B. 1999, ApJ, 514, 232
Lucke, P. B., & Hodge, P. W. 1970, AJ, 75, 171
Martín-Hernández, N. L., van der Hulst, J. M., & Tielens, A. G. G. M. 2003, A&A, 407, 957
McGee, R. X., Brooks, J. W., & Batchelor, R. A. 1972, Austr. J. Phys., 25, 581

McGee, R. X., & Milton, J. A. 1966, Austr. J. Phys., 19, 343
Mezger, P. G., & Henderson, A. P. 1967, ApJ, 147, 471
Morgan, D. H., & Good, A. R. 1985, MNRAS, 216, 459
Osterbrock, D. E. 1989, Astrophysics of gaseous nebulae and active galactic nuclei (Research supported by the University of California, John Simon Guggenheim Memorial Foundation, University of Minnesota, et al. Mill Valley, CA, University Science Books)
Panagia, N., & Walmsley, C. M. 1978, A&A, 70, 411
Parker, J. W., Garmany, C. D., Massey, P., & Walborn, N. R. 1992, AJ, 103, 1205
Rosado, M., Laval, A., Le Coarer, E., et al. 1996, A&A, 308, 588
Rudolph, A. L., Brand, J., de Geus, E. J., & Wouterloot, J. G. A. 1996, ApJ, 458, 653
Sault, R. J., Teuben, P. J., & Wright, M. C. H. 1995, in Astronomical Data Analysis Software and Systems IV, ASP Conf. Ser., 77, 4, 433
Shapley, H. 1940, Harvard College Obs. Bull., 914, 8
Shapley, H., & Lindsay, E. M. 1963, Irish Astron. J., 6, 74
Smith, L. J., Norris, R. P. F., & Crowther, P. A. 2002, MNRAS, 337, 1309
Steer, D. G., Dewdney, P. E., & Ito, M. R. 1984, A&A, 137, 159
Storm, J., Carney, B. W., Gieren, W. P., et al. 2004, A&A, 415, 531
Vacca, W. D., Garmany, C. D., & Shull, J. M. 1996, ApJ, 460, 914
Vermeij, R., Damour, F., van der Hulst, J. M., & Baluteau, J.-P. 2002, A&A, 390, 649
Wilcots, E. M. 1994a, AJ, 107, 1338
Wilcots, E. M. 1994b, AJ, 108, 1674
Wood, D. O. S., & Churchwell, E. 1989, ApJS, 69, 831